J. Fluid Mech. (1970), *vol.* 44, *part* 3, *pp.* 513–528
Printed in Great Britain

Static-pressure probes that are theoretically insensitive to pitch, yaw and Mach number

By A. M. O. SMITH AND A. B. BAUER
McDonnell Douglas Corp., Douglas Aircraft Co., Long Beach, California

(Received 5 January 1970)

The idea of distributing static probe cross-sectional areas so as to render the probe insensitive to Mach number is combined here with that of using non-circular cross-sections to render probes insensitive to yaw and angle of attack. Appropriate non-circular cross-sections are described in detail, and a general means of designing blunt or slender probes to have zero sensitivity to yaw and angle of attack in potential flow is described. Four experimental probes have been tested, and test results are presented. These results show that the probes are quite insensitive to yaw and angle of attack within certain limiting angles, which are assumed to correspond to the onset of flow separation.

1. Introduction

An ideal static-pressure probe should show the true static pressure in a fluid stream independent of the stream Mach number, Reynolds number, or direction vector. In practice this ideal is closely approached only when the Reynolds number is large, when the Mach number is not close to 1, and when the flow direction is the same as or close to the main longitudinal axis of the probe. An earlier paper (Hess & Smith 1967) describes static-pressure probe studies and testing for the case of zero angles of attack and yaw between the probe axis and the flow direction. This work was confined to probes having a circular cross-sectional shape and longitudinal area distributions derived both from subsonic theory and supersonic slender-body theory. The supersonic theory was used to design the probes from the nose back to the static-pressure hole locations. Since the area distribution downstream of these holes should not affect static pressure at the holes at supersonic speeds, subsonic theory was then used to determine the downstream area distribution such that the probes should read the true static pressure at subsonic speeds.

Faired results of numerous tests at zero angle of pitch and yaw for Mach numbers up to more than 3·0 are shown in figure 1. These results are taken from figure 8 of the Hess–Smith paper and apply to one particular round probe identified as probe VII. In addition, however, a few supersonic test values for probe IX, provided by Bauer (1969) are shown. This probe is one of the non-circular designs that forms the subject of this paper. These results demonstrate the great Mach number insensitivity. The errors indicated are mostly down in the noise level of the tests. But if the C_p errors are believed to be true, procedures

for eliminating them are straightforward and indicated briefly by Hess & Smith (1967) in a footnote. The present work makes use of the earlier longitudinal area distribution work, but utilizes non-circular cross-sectional shapes to reduce probe sensitivity to angle of attack and yaw.

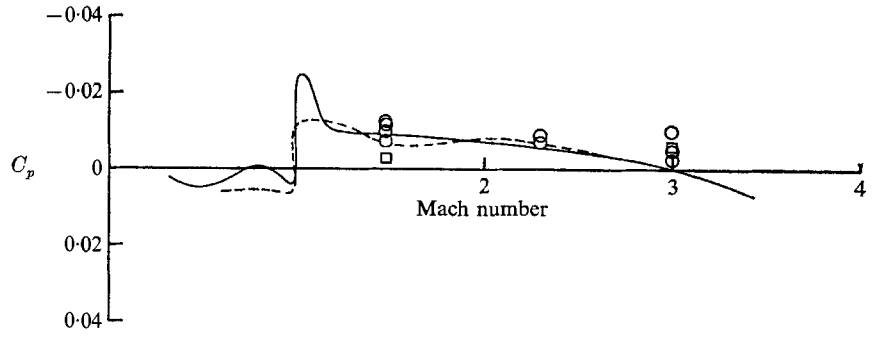

FIGURE 1. Faired results from a large number of tests in a variety of wind tunnels on probe VII, a probe of round cross-section. Probe VII: ——, pointed nose; – – –, Pitot nose. Since the probe is designed to read $C_p = 0$, C_p is just the error. Some additional test data are shown for probe IX, a probe having the same longitudinal area distribution (equation (15)) but a non-circular cross-section. Probe IX: ○○, pointed nose; □□, Pitot nose.

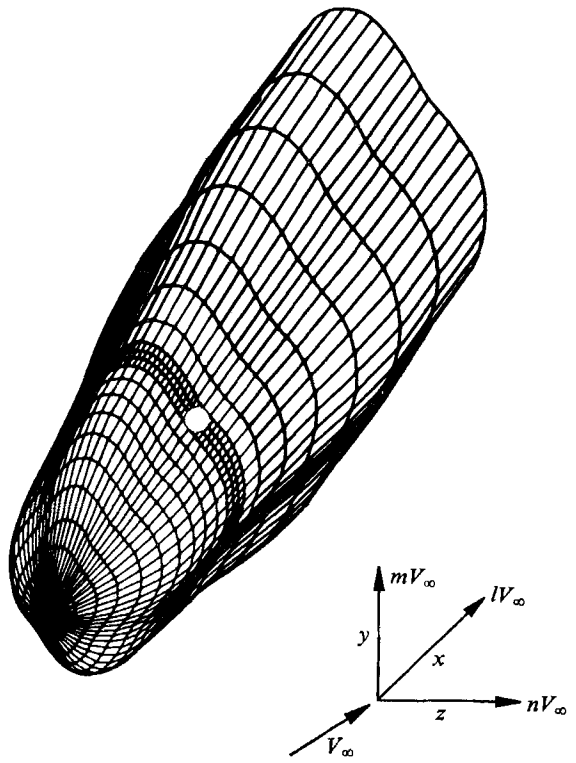

FIGURE 2. Probe XI and general co-ordinate system. The figure is an IBM 2250 perspective plot of the probe XI as defined in § 4. The white dot is an orifice location.

2. Development of probe cross-section shapes

The general probe co-ordinate system is defined in figure 2. The probe is aligned with the x axis and the relative wind direction is defined by lV_∞, mV_∞, and nV_∞, the components of the free-stream velocity V_∞ in the x, y and z directions respectively. Hence $l^2+m^2+n^2 = 1$. These components are used to define the angle of attack α and yaw β as follows:

$$\alpha = \sin^{-1} m, \quad \beta = \sin^{-1} n. \tag{1), (2)}$$

First, it is instructive to consider the problem of a very slender probe, one that is long in the x direction, so that the flow in the cross plane may be taken to be two-dimensional. Furthermore, let the cross-flow Mach numbers mV_∞/a_∞ and nV_∞/a_∞ be much less than 1 so that two-dimensional potential-flow solutions are applicable. Now if the slender body has a 'proper' area distribution $S(x)$ such that the probe pressure coefficient at the orifice or static-pressure hole cross-section plane $x = x_0$ is zero for α and $\beta = 0$ (see Hess & Smith 1967), then the probe pressure coefficient will be different from zero only because of the cross flow. For a cross-flow surface velocity V, the local pressure coefficient is

$$C_{p_l} = 1-(V^2/V_c^2), \tag{3}$$

based on the cross-flow velocity $V_c = V_\infty(m^2+n^2)^{\frac{1}{2}}$. In general, a probe may have several holes numbered 1 to s on the plane $x = x_0$; then the cross-flow pressure coefficient C_{p_c} may be defined as the average of these coefficients. This average is

$$C_{p_c} = \sum_{i=1}^{s} \frac{C_{p_{l_i}}}{s}. \tag{4}$$

Hence, for a slender probe with a proper area distribution oriented at small angles α and β to the airstream, the probe pressure coefficient based on V_c is

$$C_{p_c} = 1-\frac{1}{sV_c^2}\sum_{i=1}^{s} V_i^2. \tag{5}$$

For an ideal probe, $C_{p_c} = 0$, for all combinations of α and β. Therefore, possible probe cross-sectional shapes may be judged by this criteria. Since the simplest cross-sectional shape is the circle, this may be considered first. The surface velocity in potential flow is

$$V = 2V_\infty(m\sin\tilde{\theta}-n\cos\tilde{\theta}), \tag{6}$$

where $\tilde{\theta}$ is the angular co-ordinate $\tan^{-1}(-z/y)$, as shown in figure 3. If $n = 0$, then any combination of holes located at $\tilde{\theta} = 30°$, $150°$, $-30°$, or $-150°$ will result in $V^2 = V_c^2$ for all holes, and in $C_{p_c} = 0$. However, for an actual probe the relation (6) is modified by viscous effects such that the holes should be located in the range of $\tilde{\theta} = 30°$ to $40°$ or $-30°$ to $-40°$. Now when the cross-flow direction is changed to, say $m = 0$, and $n \neq 0$, the above suggested hole locations do not result in $C_{p_c} = 0$. With purely potential flow it is not possible with a circular cross-section to locate a set of holes such that $C_{p_c} = 0$ for arbitrary n and m. With viscous effects added, the situation is not much improved. Therefore, a search has been carried out to determine what non-circular shapes may be suitable.

Possible cross-sectional shapes may be classified by the number of pressure holes used. When configurations having one, two or three pressure holes were investigated by the authors, no suitable shapes were found. In fact, if one limits the investigation to shapes which are described by the radius vector $r(\tilde{\theta})$ such that they are symmetric in the sense that

$$r(\tilde{\theta}) = r(\tilde{\theta} + [2\pi/s]) \tag{7}$$

and

$$r(\tilde{\theta}) = r(-\tilde{\theta}), \tag{8}$$

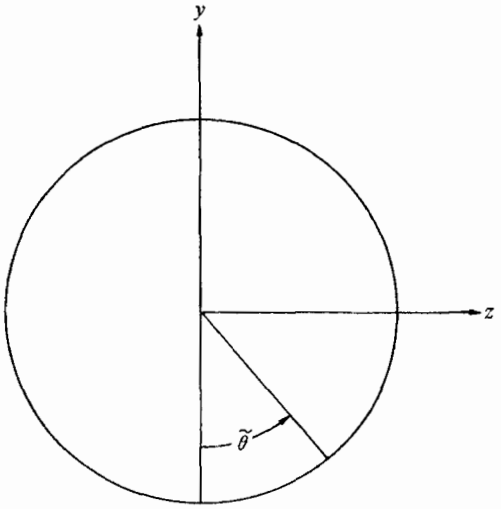

FIGURE 3. Probe cross-section showing definition of $\tilde{\theta}$.

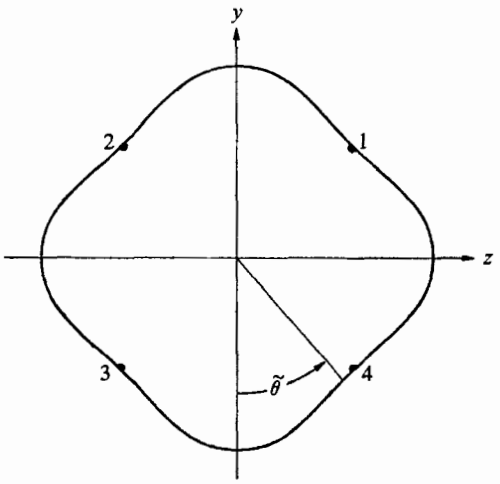

FIGURE 4. 'Rounded-square' cross-section shape, $a = 0{\cdot}1745$ (equation (9)). Dots denote pressure holes.

then it is possible to show for the potential-flow situation that no suitable shapes are possible for $s = 1$, 2, or 3. However, it can be shown that such symmetric shapes are possible for $s = 4$, 8, 12, etc. The case of $s = 4$ is illustrated in figure 4.

Since it is desirable in practice to keep the number of holes to a minimum, $s = 4$ was chosen for all the following work.

The problem of shaping can be attacked in several ways. One is as follows. Because $s = 4$, double symmetry of the shape exists. That is, the probe cross-section will have mirror symmetry about both the y and the z axis, as is illustrated by figure 4. Suppose further that the cross-sectional shape looks the same to cross-winds of either the α or the β types. Then, in order that the probe be insensitive to cross-wind velocities, the orifices must be located on 45° lines, because, whether the cross-flow component is of the α or β type, the probe appears the same to the wind. The shape then is so selected as to make $C_{p_c} = 0$ at these orifice points.

This has been done in figure 4, which illustrates the so-called 'rounded-square' shape. It is a member of the family

$$r/R = 1 - a\sin^2 2\tilde{\theta}, \tag{9}$$

where R is the maximum cross-section radius. The pressure holes are located at $\tilde{\theta} = \frac{1}{4}\pi, \frac{3}{4}\pi, \frac{5}{4}\pi$ and $\frac{7}{4}\pi$. For a cross flow in either the y or z directions (corresponding to $\beta = 0, \alpha \neq 0$ and $\alpha = 0, \beta \neq 0$, respectively) by symmetry the surface velocity squared on hole 1, V_1^2, is equal to that at the other holes, V_2^2, V_3^2 and V_4^2. When the parameter $a = 0$, $V_1^2 \to 2V_c^2$. As a increases, V_1^2 decreases. The desired value, V_1^2 equals V_c^2, was reached at $a = 0{\cdot}1745$ (Smith & Brumby 1968). This number was determined using a potential flow computer program (Hess & Smith 1966) for several values of a.

Since the above flow is potential, superposition of the flow velocities for cross flows in the y and z directions is permissible. By this means one may show that $C_{p_c} = 0$ for any combination of α and β.

Subsequently the question arose as to whether the above shape could be generalized and still satisfy the condition $C_{p_c} = 0$ for all combinations of α and β. This indeed has been found to be possible with shapes of the form

$$y/R = -(1 - a\sin^2 2\theta)\cos\theta, \tag{10}$$

$$z/R = \eta(1 - a\sin^2 2\theta)\sin\theta. \tag{11}$$

This form was written using y and z and the parameter θ rather than the radius vector $r = (y^2 + z^2)^{\frac{1}{2}}$ in order to avoid the confusion that would otherwise arise because of the fact that r points in the direction $\tilde{\theta} = \tan^{-1}(-z/y)$ rather than the θ direction. θ is related to y and z by $\theta = \tan^{-1}(-z/\eta y)$.

Such a shape is shown in figure 5 for $\eta = \frac{2}{3}$ and $a = 0{\cdot}1822$. This combination results in $C_{p_c} = 0$ for all combinations of α and β. The pressure holes had to be located at $\theta = \pm 40{\cdot}4°$ and at $\pm 139{\cdot}6°$. Figure 5 shows the section pressure distribution for cross flows in both the y and the z directions. This shape was found by systematically varying a. As a was increased, the crossover point of the V_α and V_β curves came at a more positive C_p, and vice versa. Since the V_α curve must go to $C_p = 1$ at $\theta = 180°$ and to a negative value of C_p at $\theta = 90°$ (at least for $a > 0$), and since the V_β curve must go to $C_p = 1$ at $\theta = 90°$ and to a negative value of C_p at $\theta = 180°$, the V_α and V_β curves must have a crossover

point between $\theta = 90°$ and $\theta = 180°$. Therefore, the crossover point at $C_p = 0$ might have been anticipated for some positive value of a.

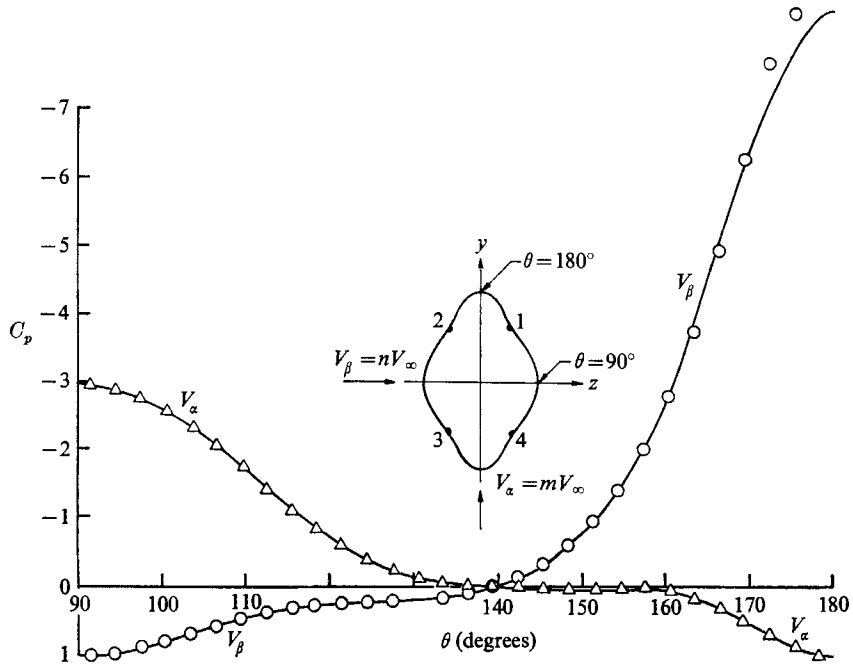

FIGURE 5. 'Rounded-diamond' cross-section shape as used on probe X. Calculated pressure coefficient distribution. θ is an angle parameter, not the polar co-ordinate. See (10) and (11). ——, two-dimensional cases; ○○△△, three-dimensional cases.

A third set of cases were computed for $\eta = \frac{1}{2}$, and the condition $a = 0{\cdot}1975$ was required for $C_{p_c} = 0$ with holes located at $\theta = \pm 37{\cdot}2°$ and $\pm 142{\cdot}8°$. The general character of the calculated pressure distributions is much like figure 5.

3. Three-dimensional probe analysis

Since the flow over practical probes is almost always three-dimensional to some degree, a three-dimensional flow analysis is useful. The analysis presented here demonstrates that probes with rather strong three-dimensional effects may be designed to read the exact static pressure for potential flows. For such flows, the numerically exact computing method of Hess & Smith (1966) has been essential for calculating probe pressure coefficients. Since numerically exact pressure calculations cannot be done in general for compressible flows, probe shapes for compressible flows must be slender so that slender-body theory can be used for the analysis.

In an actual probe viscous effects must be considered. These are not significant at small values of α and β, but can be considerable at large angles, as shown in § 5. At large angles, flow separation usually causes $\bar{C}_p$ to be negative, where $\bar{C}_p$ is defined as the average of the hole pressure coefficients. In an effort to avoid this

separation, a study was carried out to determine whether the probe orifices could be located close to the probe nose where the separation effects should be much less. Such a location brings in strong three-dimensional effects, and the probe is not slender.

The possibility that a non-slender probe may read the exact static pressure in potential flows can be studied as follows. As before, assume that the probe has four pressure holes and let u_1, v_1, w_1, be the x, y and z velocity components at hole 1. Let V_∞ be normalized to be 1. Then because of the principle of superposition of potential flow velocities we may write

$$u_1 = a_{11}l + a_{12}m + a_{13}n,$$

$$v_1 = a_{21}l + a_{22}m + a_{23}n,$$

$$w_1 = a_{31}l + a_{32}m + a_{33}n,$$

or in matrix form

$$\mathbf{V}_1 = A\mathbf{O}. \tag{12a}$$

Similarly, for the three remaining orifices

$$\mathbf{V}_2 = B\mathbf{O}, \quad \mathbf{V}_3 = C\mathbf{O}, \quad \mathbf{V}_4 = D\mathbf{O}. \tag{12b,c,d}$$

For probes of interest we require symmetry with respect to the xy and the xz planes. Because of this symmetry we can show that the components of matrices B, C and D are the same as those in A except for appropriate changes in sign. For example, figure 6 shows a probe cross-section and an onset flow component m. From the figure it is clear that the resulting v-velocity components at the four orifices are in a direction corresponding to $a_{22} = b_{22} = c_{22} = d_{22}$. It is also clear the w-velocity components are in a direction corresponding to

$$a_{32} = -b_{32} = c_{32} = -d_{32}.$$

From this type of reasoning we can show that

$$\tfrac{1}{4}(V_1^2 + V_2^2 + V_3^2 + V_4^2) = l^2V_x^2 + m^2V_y^2 + n^2V_z^2,$$

where $\mathbf{V}_x$, $\mathbf{V}_y$ and $\mathbf{V}_z$ are the three velocity vectors at any of the pressure holes for the three different flows each having $V_\infty = 1$ and having the onset direction components l, m and n equal to (1, 0, 0), (0, 1, 0) and (0, 0, 1), respectively. That is,

$$V_x^2 = a_{11}^2 + a_{21}^2 + a_{31}^2,$$

$$V_y^2 = a_{12}^2 + a_{22}^2 + a_{32}^2,$$

$$V_z^2 = a_{13}^2 + a_{23}^2 + a_{33}^2.$$

The average of the hole pressure coefficients is

$$\bar{C}_p = 1 - \tfrac{1}{4}(V_1^2 + V_2^2 + V_3^2 + V_4^2).$$

Then it follows that

$$\bar{C}_p = 1 - V_x^2 + m^2(V_x^2 - V_y^2) + n^2(V_x^2 - V_z^2). \tag{13}$$

Hence, for $V_x^2 = V_y^2 = V_z^2 = 1$ the probe will have $\bar{C}_p = 0$.

In order to design a probe to meet these conditions, there must exist three independent probe parameters that can be varied as inputs to the potential flow computing program which calculates V_x^2, V_y^2 and V_z^2. This has been done using the family of probe shapes defined by

$$y = y_1(x)\,(1 - ax^2 \sin^2 2\theta) \sin\theta, \tag{14a}$$

$$z = y_1(x)\,(1 - ax^2 \sin^2 2\theta) \cos\theta, \tag{14b}$$

where
$$y_1(x) = \frac{1}{2}\left(\frac{1-x^2}{1-ax^2+\frac{3}{8}a^2x^4}\right)^{\frac{1}{2}} \quad \text{for} \quad -1 \leqslant x \leqslant 0, \tag{14c}$$

and
$$y = \tfrac{1}{2}\sin\theta, \quad z = \tfrac{1}{2}\cos\theta \quad \text{for} \quad 0 \leqslant x. \tag{14d, e}$$

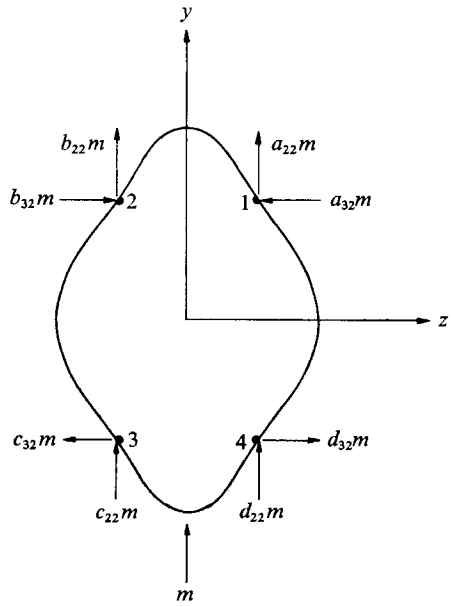

FIGURE 6. Velocity vectors at the four orifices and in the (y, z) plane generated by a y onset flow m.

In geometric terms each member of this family consists of a circular cylinder with a diameter of 1 for $x \geqslant 0$ and a modified half ellipsoid with a nose at $x = -1$ which fairs smoothly into the cylinder at $x = 0$. The ellipsoid is modified in the sense that its cross-section shape has been changed from circular to a form like that illustrated in figure 7. This cross-section shape change was accomplished without any corresponding change in the area $S(x)$. The cross-section shape can be varied through the parameter a. The four pressure-hole locations are specified by values of x_0 and θ_0. The three parameters a, x_0 and θ_0 are all that need to be varied to satisfy the conditions $V_x^2 = V_y^2 = V_z^2 = 1$.

The above family of shapes was input into the potential flow computing program with the parameter $a = 0{\cdot}45$, $0{\cdot}50$ and the $0{\cdot}465$. This last value satisfied the requirement $V_x^2 = V_y^2 = V_z^2 = 1$ for holes located at $x_0 = -0{\cdot}76$ and at $\theta_0 = \pm 45°$ and $\pm 135°$. This probe is illustrated in figure 7.

Such a blunt probe would need to be built with special care in contouring and hole location, inasmuch as $\partial \bar{C}_p/\partial x_0$ for such a blunt probe is much larger than with a slender probe. Hence, any errors in hole location will have a much larger effect on the probe reading than with a slender probe.

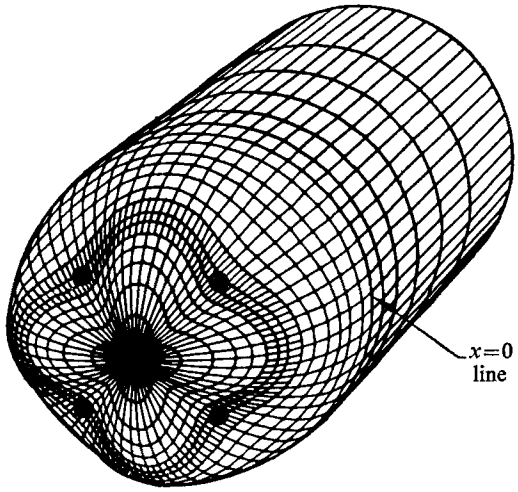

FIGURE 7. Blunt probe developed from potential flow theory with holes located near the nose. Figure is an IBM 2250 perspective plot. Black dots are orifice locations.

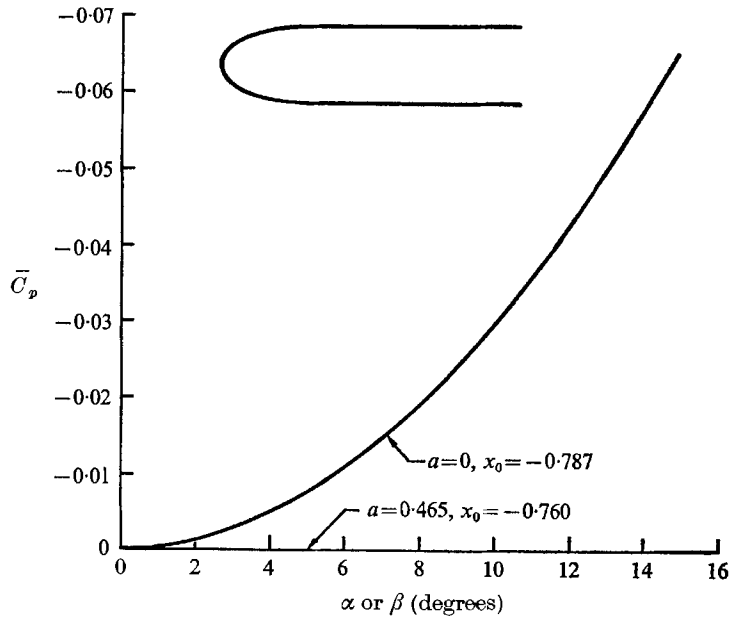

FIGURE 8. Potential flow pressure coefficients on two blunt probes; $a = 0{\cdot}465$ corresponds to the probe shown in figure 7; $a = 0$ corresponds to the related body of revolution. The profile shape sketched above has the same area distribution as both the $a = 0{\cdot}465$ and the $a = 0$ probes.

For this shape the angle between the x axis and the probe surface at the pressure holes is 33·9 degrees. Therefore the probe would be expected to operate without appreciable flow separation at much larger angles of α and β than is possible with a very slender probe.

The advantage obtained by the contouring of the blunt probe as shown in figure 7 may be better appreciated by looking at the $\bar{C}_p$ that would result if the probe were changed to a body of revolution by setting $a = 0$. Figure 8 shows $\bar{C}_p$ calculated by the method of Hess & Smith (1966) for $a = 0{\cdot}465$ and for $a = 0$. The change from 0·465 to 0 required a corresponding change in the hole station from $x_0 = -0{\cdot}760$ to $x_0 = -0{\cdot}787$. The four holes in both cases were located at $\theta_0 = \pm 45°$ and $\pm 135°$. This shows a $\bar{C}_p$ error of $-0{\cdot}0295$ for the circular probe with α or β equal to 10°.

Other blunt probe shapes are possible. For example, the ratio 2 of the ellipsoid length to diameter given by (14c) can be arbitrarily changed as long as corresponding values of a, x_0 and θ_0 can be found which result in $V_x^2 = V_y^2 = V_z^2 = 1$. Unlike the pointed slender probes, these shapes are expected to be sensitive to Mach number.

4. Experimental probes

Four experimental probes have been built and tested. These probes are much more slender than the blunt probes just discussed. Each of the experimental probes has the same area distribution $S(x)$ and length as probe VII (Hess & Smith 1967), but whereas probe VII has a circular cross-section, the newer probes have cross-sections of the form given by systematically varying the parameters in equations (10) and (11). These are given in table 1. For probe VII the angle θ_0 was optimized by extensive experimentation. On the others it is theoretical.

Probe	η	a	$\theta_{\text{pressure holes}} = \theta_0$
VII	1·0000	0·0000	±40·0°
IX	1·0000	0·1745	±45·0°, 135·0°
X	0·6667	0·1822	±40·4°, 139·6°
XI	0·5000	0·1975	±37·2°, 142·8°

TABLE 1. Probe geometric parameters

The profile equations giving the mean radii $r_a(x)$ of each of the probes are

$$r_a(x) = r_1(6{\cdot}094t^2 - 6{\cdot}281t^3 - 5{\cdot}219t^4 + 10{\cdot}406t^5 - 4{\cdot}000t^6)^{\frac{1}{2}} \quad \text{for} \quad 0 \leqslant t \leqslant 1, \tag{15a}$$

$$r_a(x) = r_1\left[1 + 0{\cdot}7\left(\frac{t-1}{1{\cdot}4}\right) + 1{\cdot}9\left(\frac{t-1}{1{\cdot}4}\right)^3 - 1{\cdot}6\left(\frac{t-1}{1{\cdot}4}\right)^4\right]^{\frac{1}{2}} \quad \text{for} \quad 1 \leqslant t \leqslant 2{\cdot}4, \tag{15b}$$

$$r_a(x) = 2^{\frac{1}{2}} r_1 \quad \text{for} \quad 2{\cdot}4 \leqslant t, \tag{15c}$$

where $t = (x/3{\cdot}125\,\text{in.}), \quad r_1 = 0{\cdot}3125\,\text{in.}, \quad S(x) = \pi r_a^2(x). \qquad (15d, e, f)$

This basic profile is illustrated in figure 9.

At any station x the mean radius r_a is related to the reference radius R of equations (10) and (11) by

$$\frac{R}{r_a} = [\eta(1 - a + \tfrac{3}{8}a^2)]^{-\frac{1}{2}},$$

which is a direct consequence of equations (10), (11), (15f) and the fact that $S(x)$ is defined as the cross-section area. Since we can take $\eta \leqslant 1$ without loss of generality, $2R$ is the major axis length of any cross-section, and $2R\eta$ is the minor axis length.

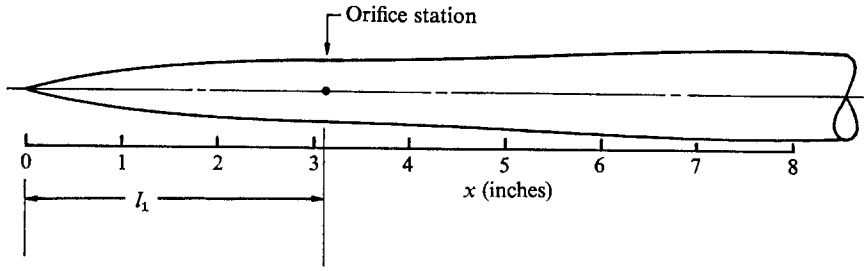

FIGURE 9. Basic probe profile used in the development of probes VII, IX, X and XI and given by equation (15). This profile is insensitive to Mach number at the orifice point according to slender-body theory.

On each of the probes the holes were located $x = l_1 = 3{\cdot}125\,\text{in.}$ from the sharp nose tip, which was located at $x = y = z = 0$. The mean diameter d_1 at the holes was $0{\cdot}625\,\text{in.}$ on each probe, giving $l_1/d_1 = 5{\cdot}0$. The pointed tips on probes X and XI were slightly rounded so that the round nose was at $x = 0{\cdot}185\,\text{in.}$

Each of the probe noses is removable, and a second nose having a Pitot tube tip can be installed instead of the plain nose. On probe IX the Pitot tip hole is $0{\cdot}187\,\text{in.}$ diameter with sharp lips which fair smoothly into the probe contour. On probes X and XI the Pitot tip holes are not round, being contoured to the probe cross-sectional shape and having mean diameters of $0{\cdot}187\,\text{in.}$ The Pitot noses were cut off at $x = 0{\cdot}437\,\text{in.}$ where the area $S(x)$ is equal to that of a $0{\cdot}187\,\text{in.}$ diameter hole so as to provide space for the Pitot holes.

On each of the probes except VII the four static pressure holes, which are each $0{\cdot}062\,\text{in.}$ in diameter, lead to a common plenum chamber inside the probe. The plenum chamber does the job of averaging the pressures from the four holes, and the plenum pressure only is measured. Probe IX was first built with separate tubes routed to each pressure hole. When the pressure readings from these four tubes were averaged mathematically and later compared with measurements using probe IX modified for plenum averaging, the two methods gave very good agreement (see Smith & Brumby 1968). This held true for pitch and yaw angles as large as 15°.

On probe VII the pressures at the two holes were measured separately and then averaged mathematically.

5. Experimental results

Probes VII and IX were tested in a subsonic stream at $M_\infty = 0{\cdot}2$ and at a Reynolds number per foot of $1{\cdot}4 \times 10^6$. Figure 10 shows $\bar{C}_p$ measured on probe VII; figure 11 shows $\bar{C}_p$ measured on probe IX. Note the very flat portions of figure 11 for $\beta = 0°$ and $\beta = 5°$ and for $-6° < \alpha < 6°$. In this region the probe cross flow does not result in a significant change in $\bar{C}_p$ with α or β. At larger angles there evidently is some boundary-layer separation, as may be judged by the well-known fact that when separation occurs it is generally on the lee side of a body where the local pressure is decreased from the potential flow value.

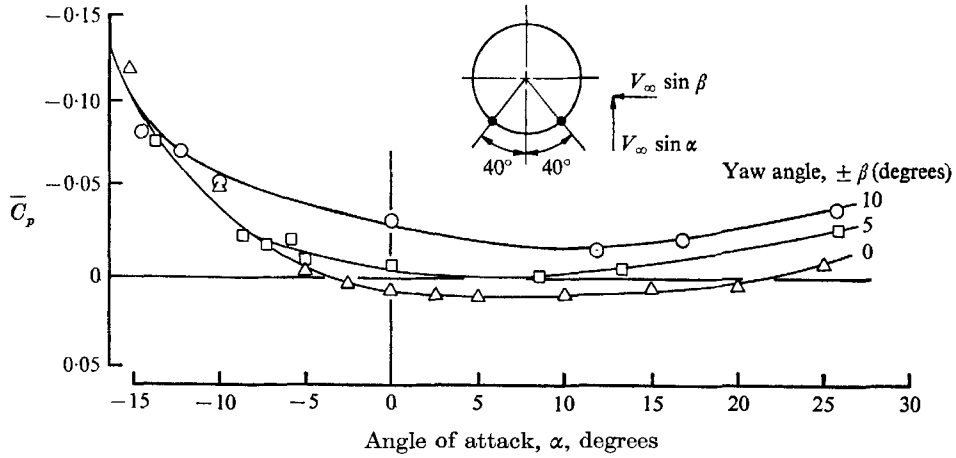

FIGURE 10. Pressure coefficients on probe VII oriented as shown with both orifices averaged together. Prove VII is the only experimental probe having a circular cross-section.

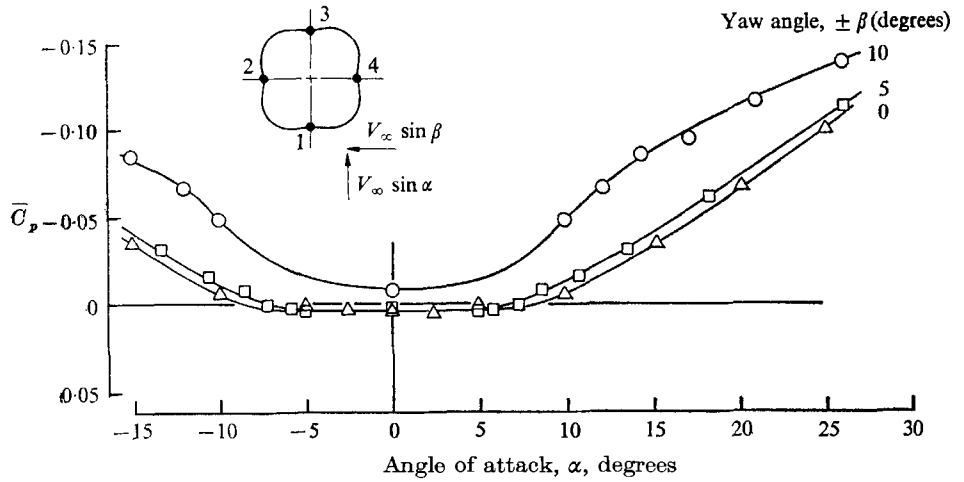

FIGURE 11. Pressure coefficients on probe IX with the pointed nose oriented as shown with all orifices averaged together.

Such a decrease appears on figure 11 as a negative $\bar{C}_p$. Note that figure 10 does not show a flat or insensitive region similar to figure 11. This demonstrates the main point of this paper—that a proper shaping of the probe cross-sections will result in very little probe sensitivity to pitch and yaw.

In figure 12 constant contours of C_{p_1} are plotted for probes VII and IX. Here C_{p_1} is defined as

$$C_{p_1} = \bar{C}_p - \bar{C}_p(\alpha = \beta = 0), \tag{16}$$

so that the figures are restricted to showing only the effects of α and β. The $\bar{C}_p$ $(\alpha = \beta = 0)$ for probe VII was discussed fully by Hess & Smith (1967); this quantity is generally quite difficult to measure with precision because the tunnel C_p is not usually known with great precision. Probes IX, X and XI are believed

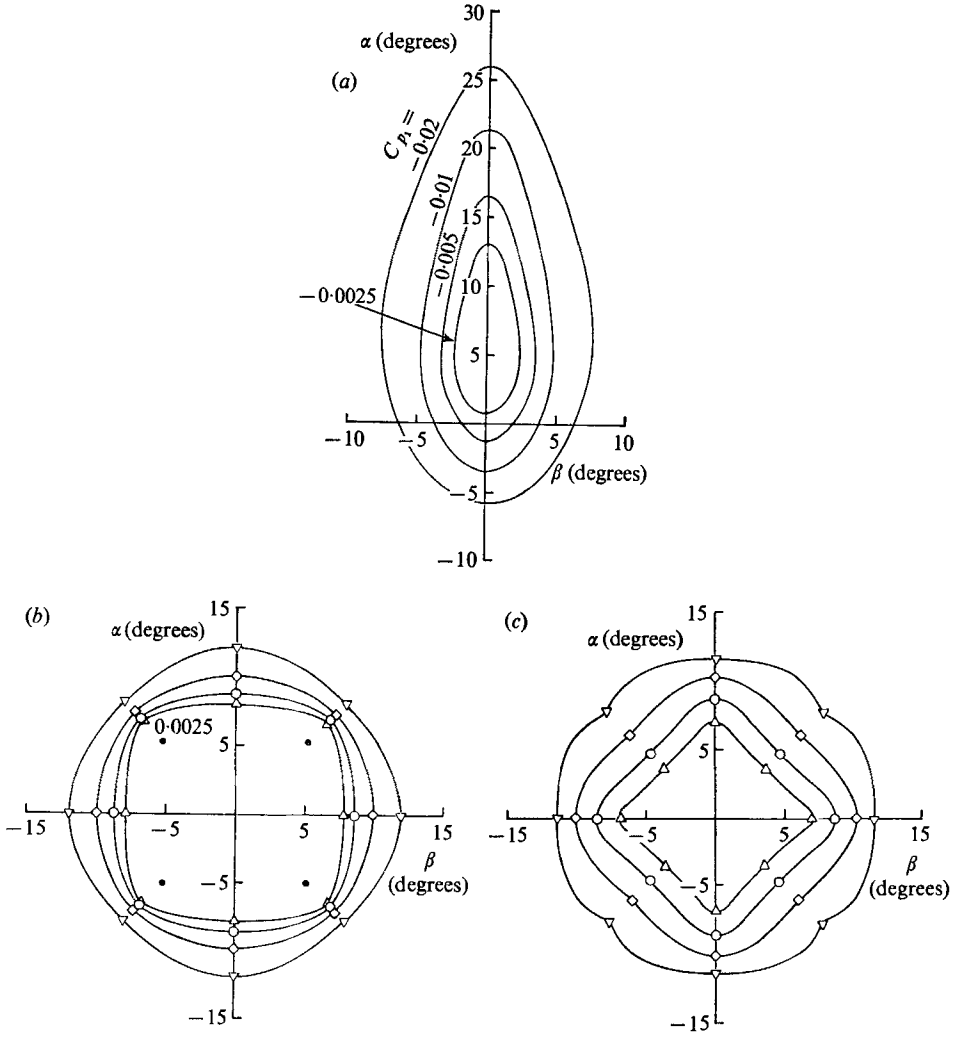

FIGURE 12. Lines of constant C_{p_1} for various probes. (*a*) Conventional probe with pointed nose (probe VII). (*b*) Probe IX with the pointed nose. (*c*) Probe IX with the Pitot nose. (*b*) & (*c*) C_{p_1}: △, −0·0025; ○, −0·005; ◇, −0·01; ▽, −0·02.

to have the same $\bar{C}_p(\alpha = \beta = 0)$ as probe VII, but only C_{p_1} will be discussed further here. Figure 12 shows clearly that probe VII is much more sensitive to β than is probe IX.

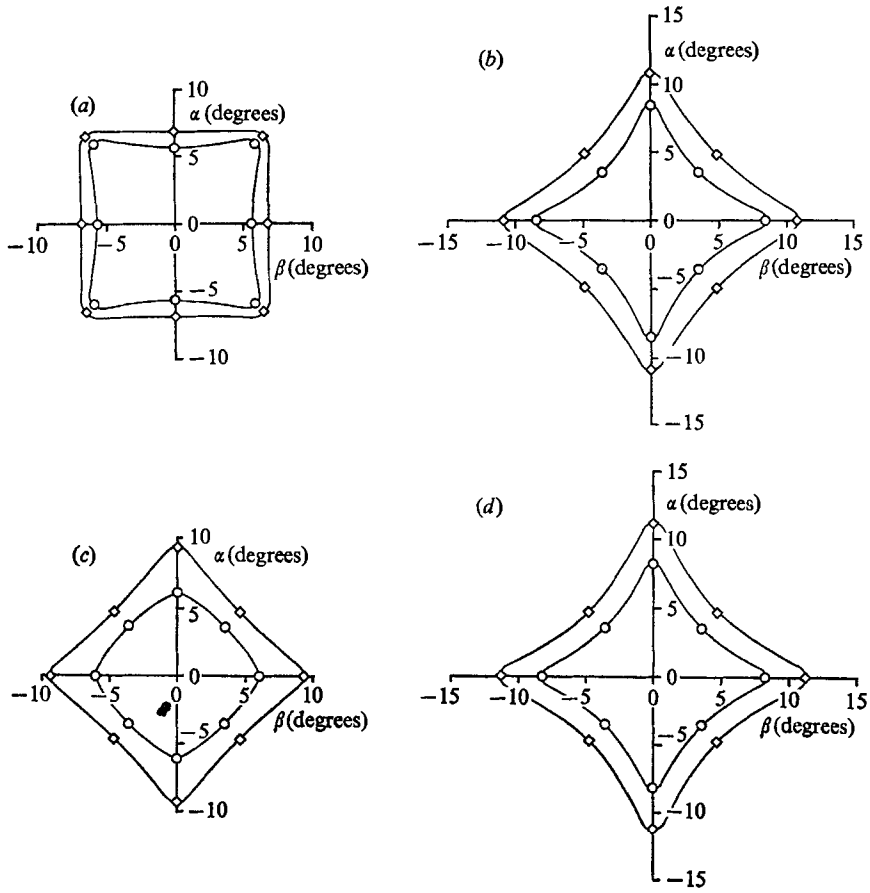

FIGURE 13. Lines of constant C_{p_1} for probe IX.
(*a*) With pointed nose $M = 1{\cdot}48$, $Re/\text{ft} = 3{\cdot}24 \times 10^6$.
(*b*) With Pitot nose $M = 1{\cdot}48$, $Re/\text{ft} = 3{\cdot}24 \times 10^6$.
(*c*) With pointed nose $M = 3{\cdot}00$, $Re/\text{ft} = 2{\cdot}17 \times 10^6$.
(*d*) With Pitot nose $M = 3{\cdot}00$, $Re/\text{ft} = 2{\cdot}17 \times 10^6$.
C_{p_1}: ○, $-0{\cdot}005$; ◇, $-0{\cdot}010$.

When probes VII and IX were operated at $M_\infty = 0{\cdot}2$ with the pointed tips, the boundary layers were laminar, as was checked using a small tube inserted into the boundary layer and attached to a stethescope. When the pointed nose was replaced by a Pitot nose on each probe, the boundary layer became turbulent, $\bar{C}_p(\alpha = \beta = 0)$ became more positive by an increment of 0·002. Contours of C_{p_1} for probe IX with the Pitot nose are shown on figure 12 (*c*).

Probe IX was also tested at $M_\infty = 1{\cdot}48$, 2·30 and 3·00 in the 2 ft Supersonic Gasdynamics Facility located at Wright–Patterson Air Force Base (Bauer 1969). Figure 13 shows C_{p_1} results at $M_\infty = 1{\cdot}48$ and 3·00; at $M_\infty = 2{\cdot}30$ intermediate

results were obtained. These results indicate only a slight increase in the sensitivity of C_{p_1} to α and β as M_∞ increases.

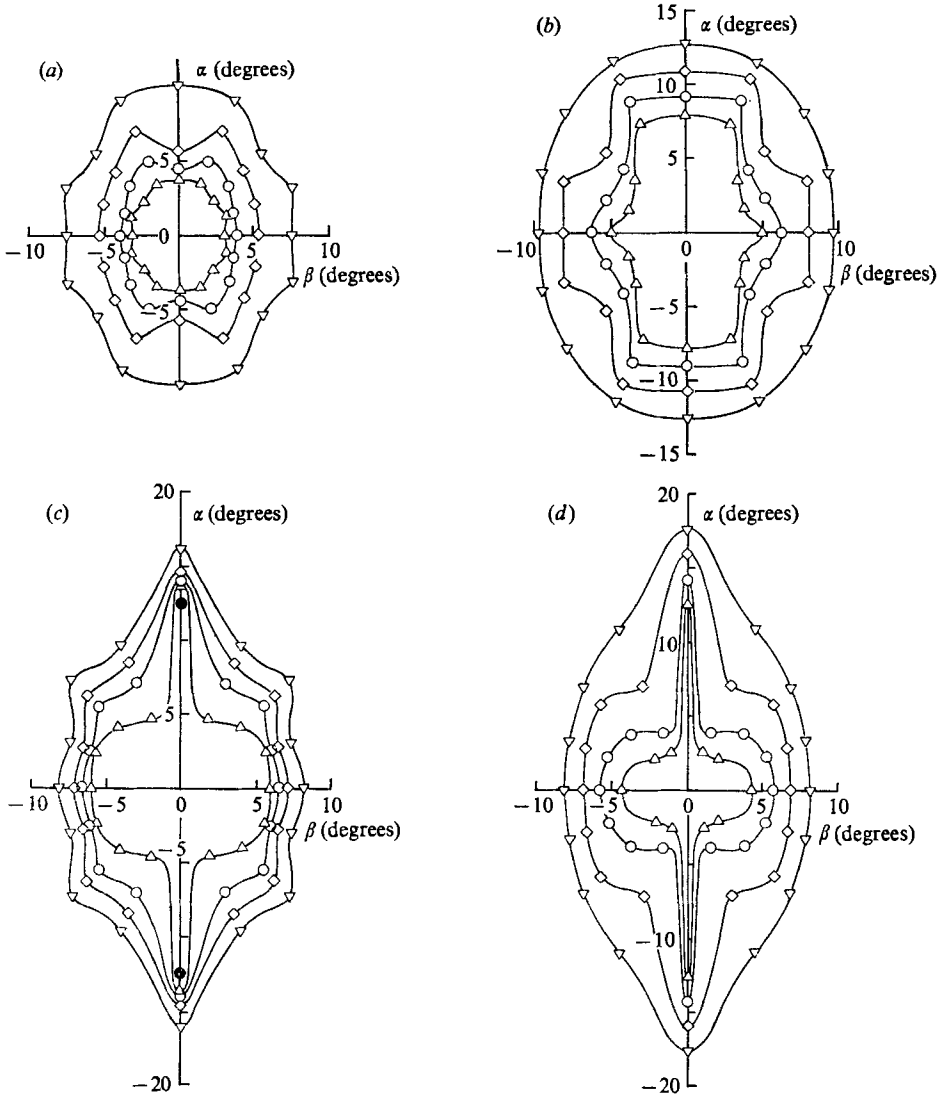

FIGURE 14. Lines of constant C_{p_1} at $M = 0{\cdot}2$. (*a*) Probe X with round nose. (*b*) Probe X with Pitot nose. (*c*) Probe XI with round nose. (*d*) Probe XI with Pitot nose. C_{p_1}: △, $-0{\cdot}0025$; ○, $-0{\cdot}005$; ◇, $-0{\cdot}01$; ▽, $-0{\cdot}02$; ●, $+0{\cdot}004$.

After the results in figure 12 had been obtained, the question arose as to whether a probe could be designed with less pitch sensitivity at the possible expense of greater sensitivity to yaw. Such a probe might find application as an aircraft static pressure sensor where yaw insensitivity is not as important as pitch insensitivity. This question resulted in the geometric design and construction of probes X and XI. The shapes were chosen in the hope that separation would be delayed to larger angles of attack than on probe IX at the expense of some

loss in yaw insensitivity. The results of probe X and XI testing at $M_\infty = 0{\cdot}2$ are shown on figure 14.

The probe X data may be compared with the similar data for probe IX on figure 12. For the rounded nose, the probe X is more sensitive to α and β than is probe IX. For the Pitot nose probe X is less sensitive than IX to α, but with respect to β IX is less sensitive than X. These Pitot nose results correspond to the results anticipated because of the probe geometries.

For probe XI the geometric change again results in a smaller sensitivity to α and a greater sensitivity to β than was the case for probe IX; this is true for both the Pitot and the rounded nose cases.

6. Conclusions

It has been shown that static pressure probes can be designed to reduce sensitivity to pitch and yaw by proper contouring of the probe cross-sections and by correct location of the pressure holes. If the probe is to operate at transonic and supersonic speeds it must be slender, but if the probe is limited to the lower subsonic speed range the probe may be blunt with the possible advantage of a further decrease in yaw and pitch sensitivity.

The authors wish to thank the Air Force Flight Dynamics Laboratory for help with tunnel testing on a co-operative programme administered by Mr Herbert A. Hutchinson, and they are appreciative of the support of the Douglas Aircraft Company through its independent research and development programme.

REFERENCES

BAUER, A. B. 1969 Supersonic test results for Douglas static probe no. IX. *McDonnell Douglas Rep.* no. DAC 67982.

HESS, J. L. & SMITH, A. M. O. 1966 Calculation of potential flow about arbitrary bodies. *Progress in Aeronautical Sciences*, **8**. Pergamon.

HESS, J. L. & SMITH, A. M. O. 1967 Static-pressure probes derived from supersonic slender-body theory. *J. Aircraft*, **4**, 409–415.

SMITH, A. M. O. & BRUMBY, R. E. 1968 A static pressure probe that is theoretically insensitive to pitch, yaw and Mach number. *McDonnell Douglas Rep.* no. DAC 66624.

Note added in proof. Recently the authors have studied the family of probe cross-section shapes defined by the polar equation $r/R = 1 - a\sin^2 4\tilde{\theta}$, so that $s = 8$ and the figure is a 'rounded octagon'. The member of this family having $a = 0{\cdot}085$ is properly indented so that a probe with the cross-section would have $\bar{C}_p = 0$ according to potential flow calculations.

Whether or not a real probe using this section is superior to the rounded square shape is not clear; in one case the adverse pressure gradients to be traversed by the boundary-layer flows are about as severe as in the other case.